2007 IEEE International Conference on
Robotics and Automation
Roma, Italy, 10-14 April 2007

Precision Control of Robots with Harmonic Drives

Wen-Hong Zhu, *Senior Member, IEEE*

***Abstract*— Aimed at achieving ultra-high precision control performance for high-end applications of robots equipped with harmonic drives, an adaptive joint torque controller developed previously is extended to all the joints of a seven degrees of freedom (DOF) robot manipulator using four different types of harmonic drives. The developed adaptive joint torque controller uses additional sensing including the joint and motor positions and the joint torque, and adaptively compensates the large friction associated with harmonic drives, while incorporating the dynamics of flexspline. With guaranteed L_2/L_∞ stability and asymptotic stability, the adaptive joint torque controller allows any motion controller to be employed. Experimental results using the developed adaptive joint torque controller incorporating a motion controller based on the *virtual decomposition control* demonstrate precision trajectory tracking control of a 7-DOF robot at both moderate and ultra-low speeds. The precision control with encoder-resolution accuracy at an ultra-low joint speed of 0.001 (rad/s) characterizes the effectiveness of the friction compensation.**

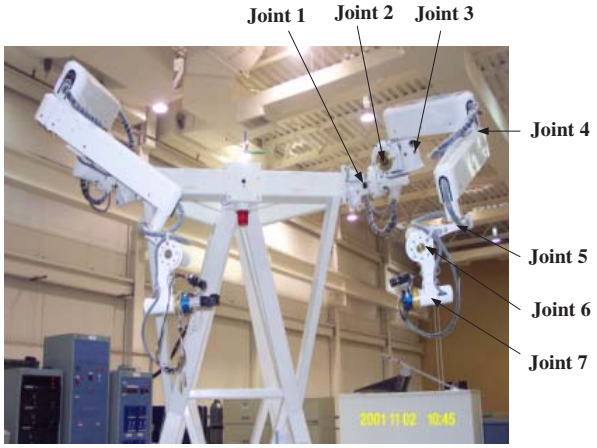

Fig. 1. Robot system.

I. INTRODUCTION

Harmonic drives are interesting for robotic applications due to their attractive properties such as high reduction ratio, compact size, lightweight and coaxial assembly. A typical harmonic drive includes a wave generator, a circular spline, and a flexspline placed in between. Being connected to the circular spline and the output shaft, the flexspline is a deformable device. This fact results in several inherent negative aspects particularly associated with the dynamics of harmonic drives, such as friction, dynamics of the flexspline, nonlinearity, and hysteresis. These negative factors dramatically challenge the control systems aimed at achieving high precision trajectory control [1]-[4].

In contrast to the input-output based linear control approaches that linearize the dynamics of harmonic drives around certain operational conditions [5], [6], the model-based dynamic control of harmonic drives has a potential of achieving precise trajectory control covering a wide range of operational conditions by exploiting the natural nonlinear dynamics of harmonic drives. Through experimental examinations of four different types of harmonic drives from HD Systems Inc., the large friction and the dynamics of the flexspline are identified as two main dynamics issues to be addressed in the control design.

To make control implementation manageable, the dynamics of the flexspline is approximately modeled as a pure torsional spring plus damping effect. However, this modeling approximation may complicate the parameter identification procedure and may even result in a big bias in parameter estimation. Therefore, adaptive control is used to automatically handle the parameter uncertainties for structured dynamics. As will be shown below, structured dynamics incorporating parameter uncertainty can be mathematically handled to deliver the L_2 and L_∞ stability and furthermore the asymptotic stability of the joint torque control.

Once the joint torque control interface performs well, most standard robot motion control algorithms that are based on joint torque control can be directly applied. In this paper, precision motion control of a robot manipulator equipped with seven harmonic drives of four different types is addressed, see Fig. 1. Joint torque control is enabled by using three measurements, namely the joint and motor positions and the joint torque, and their practically available time derivatives. The asymptotic stability of the joint torque control allows the *virtual decomposition control* [7] to be employed to realize precision motion control of robot manipulators equipped with harmonic drives at both moderate and ultra-low speeds.

This paper is organized as follows. In Section II, the dynamic model of harmonic drives is presented by taking into account the friction and the flexspline dynamics. In Section III, an adaptive joint controller originally developed in [8] is extended to all the joints of a robot to ensure joint torque tracking control. Based this adaptive joint torque controller, the *virtual decomposition control* [7], [9] is applied in Section IV. In Section V, experimental results on precision motion control of a 7-joint robot manipulator equipped with harmonic drives are demonstrated. The precision control result at an ultra-low speed confirms the effectiveness of the friction compensation.

The author is with the Spacecraft Engineering, Space Technologies, Canadian Space Agency, 6767 route de l'Aeroport, Saint-Hubert, QC J3Y 8Y9, Canada (e-mail: Wen-Hong.Zhu@space.gc.ca)

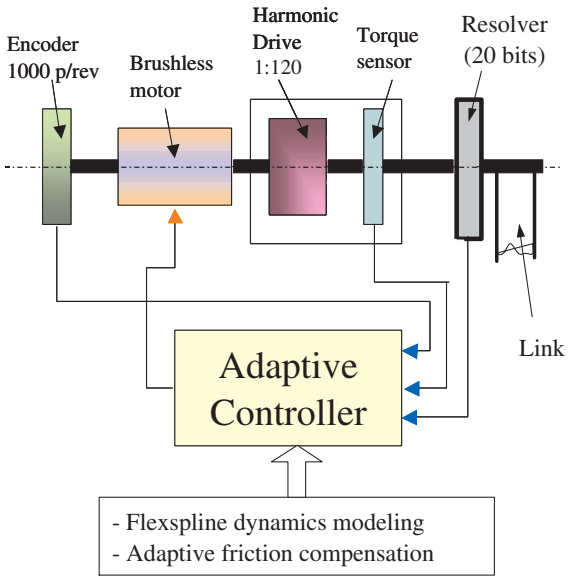

Fig. 2. Joint assembly with harmonic drive and controller.

II. HARMONIC DRIVE DYNAMICS

A typical harmonic drive consists of a wave-generator that is connected to the motor, a circular spline that is connected to the base, and a flexspline that is placed in between and connected to the joint [1]. The flexspline is a deformable device and is modeled as a pure torsional spring with damping effect.

Fig. 2 illustrates a joint assembly with harmonic drive and controller. For each harmonic drive, four pairs of strain gauges are mounted on the flexspline by using the approach in [10], [11]. The outputs of the four pairs of strain gauges create the joint torque measurement. Meanwhile, an encoder is mounted at the motor side and a resolver is mounted at the joint side. All three (two positions and one torque) measurements are fed to the adaptive joint torque controller to make sure that the measured torque tracks the desired or required torque computed from a motion controller asymptotically.

The dynamic equation of a harmonic drive assembled with a DC motor can be written as

$$k_f[d(\dot{\phi}-\dot{q})+(\phi-q)] = \tau \quad (1)$$

$$I^*\ddot{\phi}+f_\phi(\dot{\phi},\tau)+k_f[d(\dot{\phi}-\dot{q})+(\phi-q)] = u+u_d \quad (2)$$

where τ denotes the physical torque passing through the flexspline; $k_f>0$ is the stiffness of the flexspline; ϕ is the angle of the motor rotor divided by the gear ratio; q is the joint angle; $dk_f>0$ represents the damping coefficient of the flexspline; I^* denotes the rotor inertia of the DC motor multiplied by the gear ratio squared; $f_\phi(\dot{\phi},\tau)$ denotes the frictional torque that is assumed to be a function of the motor rotor velocity and the payload; u is the motor driving torque multiplied by the gear ratio; and $u_d\in L_\infty$ denotes the disturbance torque caused by external disturbances.

Remark 2.1: Introducing damping effect into the flexspline dynamics can be found in [12] and recently in [13]. In case of $d=0$, (1) and (2) are equivalent to the dynamics of a flexible joint [9], [14], [15].

The model of the frictional torque $f_\phi(\dot{\phi},\tau)$ takes the Coulomb and viscous effects into account, and is expressed as

$$f_\phi(\dot{\phi},\tau) = \begin{cases} g(\tau)k_c+c+k_{vp}\dot{\phi} & \dot{\phi}>0 \\ [-g(\tau)k_c, g(\tau)k_c]+c & \dot{\phi}=0 \\ -g(\tau)k_c+c+k_{vn}\dot{\phi} & \dot{\phi}<0 \end{cases}$$
$$\stackrel{def}{=} Y_\phi(\dot{\phi},\tau)\theta \quad (3)$$

where $k_c>0$ denotes the magnitude of the Coulomb torque at zero payload and $c>0$ denotes a DC offset. Introducing the DC offset c in the friction model allows the Coulomb friction to have different values at positive and negative velocities; $k_{vp}>0$ and $k_{vn}>0$ denote the viscous friction coefficients at positive and negative velocities, respectively;

$$g(t)\stackrel{def}{=}1+g_1\mid\tau\mid+g_2\mid\tau\mid^2 \quad (4)$$

with $g_1>0$ and $g_2>0$ is a function used to emulate the load dependent Coulomb friction effect[1]; and

$$\theta=\begin{bmatrix} k_c & c & k_{vp} & k_{vn}\end{bmatrix}^T\in R^4$$

represents the uncertain parameter vector, and $Y_\phi(\dot{\phi},\tau)\in R^{1\times 4}$ represents the corresponding regressor matrix.

III. ADAPTIVE JOINT TORQUE CONTROL

The adaptive joint controller originally developed in [8] is extended to all the joints of a seven-DOF robot. For each joint, the control algorithms are summarized as

$$F(s)\stackrel{def}{=}\frac{1}{ds+1} \quad (5)$$

$$\zeta\stackrel{def}{=}\frac{1}{k_f} \quad (6)$$

$$\phi_d = q+F(s)\hat{\zeta}\tau_r \quad (7)$$

$$\dot{\phi}_r = \dot{\phi}_d+\lambda_\phi(\phi_d-\phi)+\lambda_\tau(\tau_r-\tau) \quad (8)$$

$$u = I^*\ddot{\phi}_r+\hat{f}_\phi(\dot{\phi}_r,\tau)+k_\phi(\dot{\phi}_r-\dot{\phi}) +\tau_r+k_\tau(\tau_r-\tau) \quad (9)$$

to realize joint torque control, where $\tau_r\in L_\infty$ represents the required torque coming from the output of a motion controller with $\dot{\tau}_r\in L_\infty$; $\hat{\zeta}$ denotes the estimate of ζ defined by (6); $\lambda_\phi>0$, $\lambda_\tau>0$, $k_\phi>0$, and $k_\tau>0$ are control gains; and

$$\hat{f}_\phi(\dot{\phi}_r,\tau)=Y_\phi(\dot{\phi}_r,\tau)\hat{\theta}. \quad (10)$$

The parameter estimates $\hat{\theta}$ and $\hat{\zeta}$ are updated in real-time by using the $\mathcal{P}$ function defined in [9] (page 311) as

$$\hat{\theta}_i = \mathcal{P}(s_i(t),\rho_i,\theta_i^-,\theta_i^+) \quad (11)$$

$$\hat{\zeta} = \mathcal{P}(s_\zeta(t),\rho_\zeta,\zeta^-,\zeta^+) \quad (12)$$

[1]Fig. 1 in [8] shows a payload dependent Coulomb friction profile for harmonic drive CSF-45-120-2A-GR from HD Systems Inc. It shows that the Coulomb friction at a payload of 1000 (Nm) is almost about 7 $\sim$ 8 times higher than that without payload.

where $\hat{\theta}_i$ denotes the ith element of $\hat{\theta}$, $i = 1, 2, 3, 4$; $\rho_i > 0$ is an update gain; θ_i^- and θ_i^+ denote the lower and upper bounds of the ith element of θ; and $s_i(t)$ denotes the ith element of $s(t) \in R^4$ defined by

$$s(t) = (\dot{\phi}_r - \dot{\phi}) Y_\phi(\dot{\phi}_r, \tau)^T. \quad (13)$$

Accordingly, $\rho_\zeta > 0$ is an update gain; ζ^- and ζ^+ denote the lower and upper bounds of ζ; and $s_\zeta(t)$ is governed by

$$s_\zeta(t) = -(1 + k_\tau)\tau_r \left[(\dot{\phi}_d - \dot{\phi}) + \lambda_\phi (\phi_d - \phi) \right]. \quad (14)$$

Remark 3.1: In view of (8) and (9), $\ddot{\phi}_r$ in u is a linear function of $\dot{\tau}$, and so is u. On the other hand, $\ddot{\phi}$ is a linear function of u in view of (2), and $\dot{\tau}$ is a linear function of $\ddot{\phi}$ in view of (1). Thus, an algebraic loop involving $\dot{\tau}$, $\ddot{\phi}_r$, u, and $\ddot{\phi}$ is formed in view of (1), (2), (8), and (9). A necessary and sufficient condition to ensure the stability of this algebraic loop in discrete-time implementation is $k_f d \lambda_\tau < 1$, which imposes a limitation on λ_τ in (8). Note that the algebraic loop is formed by including a damping coefficient d in the dynamic model (1) and (2). In other words, if the damping effect is negligible as in the cases of [9], [14], [15], no algebraic loop exists. By using a close estimation of $d = 0.001$ (s), a stiffness $k_f = 2.9 \times 10^5$ (Nm/rad), and a control parameter $\lambda_\tau = 0.0002$ (1/Nms), it yields $k_f d \lambda_\tau = 0.058 < 1$. The necessary and sufficient condition to ensure the stability of the algebraic loop is satisfied.

The theoretical results are summarized in a theorem.

Theorem 1: Consider a harmonic drive described by (1)-(4) combined with the adaptive joint torque control described by (5)-(14). It follows that

i)

$$\int_0^T (\dot{\phi}_r - \dot{\phi})^2 dt \leq \frac{1}{k_\phi^2} \int_0^T u_d^2 dt + \frac{2}{k_\phi} V_1(0) \quad (15)$$

$$\int_0^T (\phi_d - \phi)^2 dt \leq \frac{1}{2k_\phi(1 + k_\tau)\lambda_\phi k_f} \int_0^T u_d^2 dt + \frac{1}{(1 + k_\tau)\lambda_\phi k_f} V_1(0) \quad (16)$$

$$\int_0^T (\dot{\phi}_d - \dot{\phi})^2 dt \leq \frac{1}{2k_\phi(1 + k_\tau) d k_f} \int_0^T u_d^2 dt + \frac{1}{(1 + k_\tau) d k_f} V_1(0) \quad (17)$$

$$\int_0^T (\tau_r - \tau)^2 dt \leq \frac{1}{2k_\phi(1 + k_\tau)\lambda_\tau} \int_0^T u_d^2 dt + \frac{1}{(1 + k_\tau)\lambda_\tau} V_1(0) \quad (18)$$

with $V_1(0) \geq 0$;

ii)

$$\dot{\phi}_r - \dot{\phi} \in L_2 \quad (19)$$
$$\dot{\phi}_d - \dot{\phi} \in L_2 \quad (20)$$
$$\phi_d - \phi \in L_2 \quad (21)$$
$$\tau_r - \tau \in L_2 \quad (22)$$

if $u_d \in L_2$;

iii)

$$\dot{\phi}_r - \dot{\phi} \in L_\infty \quad (23)$$
$$\dot{\phi}_d - \dot{\phi} \in L_\infty \quad (24)$$
$$\phi_d - \phi \in L_\infty \quad (25)$$
$$\tau_r - \tau \in L_\infty \quad (26)$$

if $\tau_r \in L_\infty$; and

iv)

$$\dot{\phi}_r - \dot{\phi} \to 0 \quad (27)$$
$$\dot{\phi}_d - \dot{\phi} \to 0 \quad (28)$$
$$\phi_d - \phi \to 0 \quad (29)$$
$$\tau_r - \tau \to 0 \quad (30)$$

if $u_d \in L_2$, $\tau_r \in L_\infty$, $\dot{\tau}_r \in L_\infty$, and $\dot{q} \in L_\infty$. ■

The proof can be found in [8].

Remark 3.2: It can be verified that all stability results in Theorem 1 are still valid for $d = 0$ in (1) and (2). Therefore, the adaptive joint torque controller is compatible with the dynamic model in which only the torsional stiffness is considered as in [9], [14], [15]. Importantly, in case of $d = 0$, the algebraic loop described in *Remark 3.1* is non-existent.

IV. ROBOT MOTION CONTROL

As far as joint position control of a seven-joint robot manipulator as illustrated in Fig. 1 is concerned, the seven joints are numbered sequentially from the base toward the tip, with joint j connecting link j with link $j - 1$. Seven frames, $\{L_j\}$, $j \in \{1, 7\}$, are formed in a way that frame $\{L_j\}$ is fixed to link j with its z axis coincident with the jth joint axis.

Given $\tau_j \to \tau_{jr}$, $j \in \{1, 7\}$, the motion control objective is to find τ_{jr} such that $q_j \to q_{jd}$, $j \in \{1, 7\}$.

Given reference signals q_{jd}, $\dot{q}_{jd}$, and $\ddot{q}_{jd}$, the *virtual decomposition control* algorithm in [9] is summarized in this section.

First, the required joint velocities and accelerations are obtained as

$$\dot{q}_{jr} = \dot{q}_{jd} + \lambda_j (q_{jd} - q_j) \quad (31)$$
$$\ddot{q}_{jr} = \ddot{q}_{jd} + \lambda_j (\dot{q}_{jd} - \dot{q}_j) \quad (32)$$

where $\lambda_j > 0$ is a constant.

Let ${}^{L_j}X \in \Re^6$ be the linear/angular velocities of frame $\{L_j\}$, and expressed in frame $\{L_j\}$, and let ${}^{L_j}F \in \Re^6$ be the force/moment measured and expressed in frame $\{L_j\}$. Moreover, let ${}^{L_j}U_{L_{j+1}} \in \Re^{6\times 6}$ be a force/moment transformation matrix that transfers a force/moment vector measured and expressed in frame $\{L_{j+1}\}$ to the same force/moment measured and expressed in frame $\{L_j\}$.

Thus, the linear/angular velocities of all seven links are computed as

$${}^{L_j}X = Z\dot{q}_j + {}^{L_{j-1}}U_{L_j}^T \, {}^{L_{j-1}}X \quad (33)$$

for $j = 1, 2, \cdots, 7$ with $Z = [0, 0, 0, 0, 0, 1]^T$ and ${}^{L_0}X = 0$.

Accordingly, the required linear/angular velocities of all seven links are computed as

$$^{L_j}X_r = Z\dot{q}_{jr} + {}^{L_{j-1}}U_{L_j}^T\, {}^{L_{j-1}}X_r \tag{34}$$

for $j = 1, 2, \cdots, 7$ with $Z = [0, 0, 0, 0, 0, 1]^T$ and $^{L_0}X_r = 0$. Differentiating (34) with respect to time yields $\frac{d}{dt}\left(^{L_j}X_r\right)$ for $j = 1, 2, \cdots, 7$. Define

$$Y_{L_j}\theta_{L_j} = M_{L_j}\frac{d}{dt}\left(^{L_j}X_r\right) + C_{L_j}(^{L_j}\omega)^{L_j}X_r + G_{L_j} \tag{35}$$

for $j \in \{1, 7\}$, where $M_{L_j} \in \Re^{6\times 6}$, $C_{L_j}(^{L_j}\omega) \in \Re^{6\times 6}$, and $G_{L_j} \in \Re^6$ are two matrices and one vector representing the dynamic properties of link j with their detailed expressions given in [7]. In (35), $Y_{L_j} \in \Re^{6\times 13}$ is a regressor matrix and $\theta_{L_j} \in \Re^{13}$ is the dynamic parameter vector[2] of link j.

The required net forces/moments of all links are computed as

$$^{L_j}\underline{F}_r = Y_{L_j}\hat{\theta}_{L_j} \tag{36}$$

for $j \in \{1, 7\}$, where the parameter estimate vector $\hat{\theta}_{L_j} \in \Re^{13}$ is used in lieu of the true parameter vector $\theta_{L_j} \in \Re^{13}$. Define

$$\psi_{L_j} = Y_{L_j}^T\left(^{L_j}X_r - {}^{L_j}X\right). \tag{37}$$

The γth element of $\hat{\theta}_{L_j} \in \Re^{13}$ is updated by

$$\hat{\theta}_{L_j\gamma} = \mathcal{P}\left(\psi_{L_j\gamma}, \rho_{L_j\gamma}, \theta^-_{L_j\gamma}, \theta^+_{L_j\gamma}\right) \tag{38}$$

for $\gamma \in \{1, 13\}$, where $\psi_{L_j\gamma}$ denotes the γth element of ψ_{L_j}, $\rho_{L_j\gamma} > 0$ is an update gain, $\theta^-_{L_j\gamma}$ and $\theta^+_{L_j\gamma}$ denote the lower and upper bounds of the γth element of $\theta_{L_j} \in \Re^{13}$.

After obtaining $^{L_j}\underline{F}_r \in \Re^6$, $j \in \{1, 7\}$, the required forces/moments at frames $\{L_j\}$, $j \in \{1, 7\}$, are computed as

$$^{L_j}F_r = {}^{L_j}\underline{F}_r + {}^{L_j}U_{L_{j+1}}\, {}^{L_{j+1}}F_r \tag{39}$$

for $j = 7, 6, \cdots, 1$ with $^{L_8}F_r = 0$.

Finally, the required joint torques are computed as

$$\tau_{jr} = Z^T\, {}^{L_j}F_r + k_{pj}(\dot{q}_{jr} - \dot{q}_j) + \mathcal{P}\left(\dot{q}_{jr} - \dot{q}_j, k_{Ij}, t^-_{sj}, t^+_{sj}\right) \tag{40}$$

with $k_{pj} > 0$, $k_{Ij} > 0$, $t^-_{sj} < 0$, and $t^+_{sj} > 0$, for $j \in \{1, 7\}$.

Theorem 2: Consider a seven-joint serial-link robot manipulator subjected to the *virtual decomposition control* described by (31)-(40), under bounded reference signals q_{jd}, $\dot{q}_{jd}$, $\ddot{q}_{jd}$, $j \in \{1, 7\}$, and asymptotic joint torque tracking control $\tau_j \to \tau_{jr}$, $j \in \{1, 7\}$. It follows that

$$q_{id} - q_i \;\to\; 0 \tag{41}$$

$$\dot{q}_{id} - \dot{q}_i \;\to\; 0. \tag{42}$$

■

The proof can be found in [9].

[2]There exist three dependent parameters in θ_{L_j}, in order to express (35) in a linear-in-parameter form.

V. EXPERIMENTS

The adaptive joint torque controller incorporating the *virtual decomposition control* is experimentally verified on a seven-joint redundant robot manipulator, see Fig. 1. Four different types of harmonic drives as listed in Table I are tested with respect to the proposed control approach. The control gains associated with the adaptive joint torque controller described by (5)-(14) and the virtual decomposition base motion controller described by (31)-(40) are listed in Table II.

The QNX based real-time operating system with RT-LAB from OPL-RT is adopted as a main platform for control computation with a sampling rate of 1000 Hz.

In view of (5)-(9), the variables required for implementing the control torque u include the joint position q, velocity $\dot{q}$, and acceleration $\ddot{q}$; the motor position ϕ and velocity $\dot{\phi}$; the joint torque τ and its derivative $\dot{\tau}$; and the required torque τ_r and its derivative $\dot{\tau}_r$. In the implementation, only q, ϕ, and τ are taken directly from the measurements. The remaining variables $\dot{q}$, $\ddot{q}$, $\dot{\phi}$, and $\dot{\tau}$ are generated numerically by using $s \Rightarrow s\frac{200}{s+200} \Rightarrow \frac{200(z-1)}{z-0.8}$, where a low-pass filter with a cut-off frequency of 200 (rad/s) is added and $s = \frac{z-1}{T}$ with $T = 0.001$ (s) is applied. For instance, the resolver in Joint 7 gives a $2\pi/2^{16} \approx 9.6 \times 10^{-5}$ (rad) resolution for q, which is equivalent to a $9.6 \times 10^{-5} \times 200^2 \approx 3.8$ $(\mathrm{rad/s^2})$ resolution for $\ddot{q}$. In view of $I^* = 1.0$ $(\mathrm{Nms^2})$, it yields a 3.8 (Nm) torque resolution for the control. The maximum continuous torque for Joint 7 is $0.63\times 160 = 100.8$ (Nm). Thus, the numerical differentiation induced torque ripple takes less than 4% of the maximum continuous control torque. On the other hand, use of the derivative of the measured torque introduces $I^*\lambda_\tau \times 200 \approx 0.04$ ($\lambda_\tau = 0.0002$ is used) times torque measurement noise into the control torque for Joint 7. The same analysis applies to the other joints. In summary, the use of high order derivatives of the measurement variables through numerical differentiation only introduces an acceptable level of noise to the control torque.

In [8], the joint torque controller incorporating a simple motion controller was experimentally tested with respect to a particular harmonic drive located at Joint 7. The feasibility of the controller was witnessed by extensive experimental results for both joint torque control and joint position control presented in both time and frequency domains. Quantitative experimental analysis with respect to both friction compensation and flexspline dynamics based control was given.

In this paper, the adaptive joint torque controller is extended to all seven joints of a robot manipulator equipped with harmonic drives, and is being used together with the *virtual decomposition control* for achieving precision motion control. Experimental results are presented with respect to both individual joint motion and coordinated joint motion.

The experimental results for individual joint motion conducted on Joints 3, 4, 5, and 7, respectively, under different sinusoidal inputs are summarized in Table III.

Coordinated joint motion at both moderate and ultra-low

TABLE I

HARMONIC DRIVE AND MOTOR PARAMETERS.

	Motor	**Harmonic drive**	**Gear ratio**	**Stiffness** (Nm/rad)
Joints 1-3	RBEH-3002	CSF-45-120-2A-GR	120	2.9×10^5
Joint 4	RBEH-2103	CSF-32-120-2A-GR	120	1.1×10^5
Joints 5-6	RBEH-1503	CSF-25-160-2A-GR	160	5.0×10^4
Joint 7	RBEH-1503	CSF-20-160-2A-GR	160	2.6×10^4

TABLE II

CONTROL PARAMETERS FOR JOINT TORQUE CONTROL.

	Joints 1-3	**Joint 4**	**Joints 5-6**	**Joint 7**
d (s)	0.001	0.001	0.001	0.001
λ_ϕ (1/s)	50	45	50	50
λ_τ (1/Nms)	0.0002	0.0002	0.0002	0.0002
I^* (Nms^2)	28*	5	2.1	1.0
k_ϕ (Nms)	500	200	100	25
k_τ	0	0.8	0.75	1.0
ρ_1 (Nm)	2000	2000	1000	400
θ_1^- (Nm)	-35	-5	-4	-4
θ_1^+ (Nm)	35	5	4	7
ρ_2 (Nm)	10000	200	100	100
θ_2^- (Nm)	-200	-50	-20	-10
θ_2^+ (Nm)	200	50	20	10
ρ_3 (Nms^2)	50000	30000	50000	40000
θ_3^- (Nms)	0	0	0	0
θ_3^+ (Nms)	700	90	90	80
ρ_4 (Nms^2)	50000	30000	50000	40000
θ_4^- (Nms)	0	0	0	0
θ_4^+ (Nms)	700	90	90	80
ρ_ζ ($1/(\mathrm{Nm})^2$)	1.0×10^{-6}	1.0×10^{-5}	1.0×10^{-4}	1.0×10^{-4}
ζ^- (1/Nm)	2.5×10^{-6}	7×10^{-6}	1.5×10^{-5}	3.0×10^{-5}
ζ^+ (1/Nm)	3.5×10^{-6}	1.0×10^{-5}	2.5×10^{-5}	4.0×10^{-5}
λ (1/s)	25	45	30	30
k_p (Nms)	2000	500	100	80
k_I (Nm)	25000	4000	2000	2000
t_s^- (Nm)	-400	-200	-100	-50
t_s^+ (Nm)	400	200	100	50

$*$ The value used in the controller may be different from the physical value.

TABLE III

POSITION CONTROL PERFORMANCES FOR INDIVIDUAL JOINTS.

	Frequency (Hz)	**Amplitude** (rad)	**Maximum joint position error** (rad)
Joint 3	0.5	0.1	0.0004
	2.0	0.02	0.0021
Joint 4	0.5	0.1	0.0005
	2.0	0.02	0.0020
Joint 5	0.5	0.1	0.0006
	2.0	0.02	0.0020
Joint 7	0.5	0.15	0.0008
	5.0	0.015	0.0033

speeds are also tested. All seven joints of the robot move simultaneously with an increment of 10 deg. for each joint. The control performance at a moderate speed witnesses the controller capability of handling the dynamic interactions not only among the multiple joints but also between the joint torque control and the motion control. The control performance at an ultra-low speed particularly demonstrates the effectiveness of the joint friction compensation. Figs. 3 and 4 demonstrate the position tracking control results of Joint 3 at both moderate and ultra-low speeds[3]. The maximum joint trajectory tracking errors are 4.88×10^{-4} (rad) = 1.68 arc-min[4] at a moderate speed of 0.4 (rad/s), and 4.48×10^{-5} (rad) = 0.154 arc-min[5] at an ultra-low speed of 0.001 (rad/s). In Fig. 4, no stick-slip behavior is observed, which demonstrates the feasibility of the adaptive joint friction compensation.

Remark 4.1: Like most direct adaptive control approaches, it is unnecessary to have parameter estimates converged to

[3]Results for other joints have a similar profile. They are not presented here for saving space.

[4]This result is comparable to the result of individual joint movement of Joint 3 at Row 1 of Table III, where the maximum joint position error is 4×10^{-4} (rad) at a maximum speed of 0.314 (rad/s). The similarity of position tracking errors between individual joint movement and coordinated robot movement reveals the effectiveness of the *virtual decomposition control* that handles robot linkage dynamics.

[5]This value reaches the scale of the encoder resolution of $2\pi/(4 \times 1000 \times 120) = 1.3 \times 10^{-5}$ (rad).

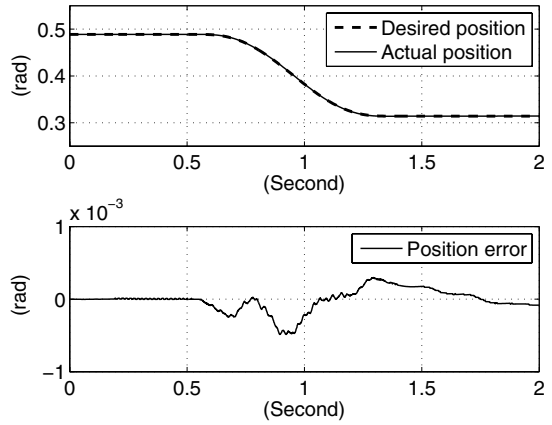

Fig. 3. Joint 3 position tracking result for a coordinated all-joint movement at a moderate speed of 0.4 (rad/s). The dashed line is the designed trajectory and the solid line is the actual joint position.

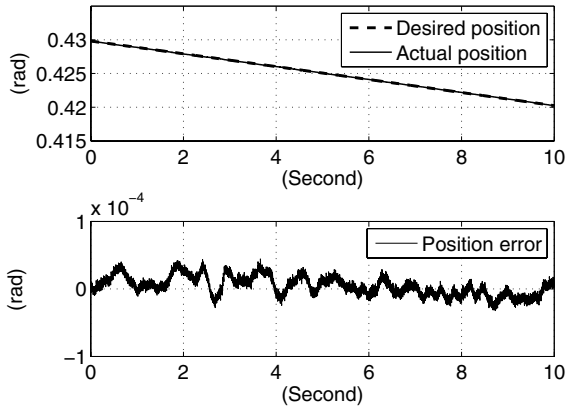

Fig. 4. Joint 3 position tracking result for a coordinated all-joint movement at an ultra-low speed of 0.001 (rad/s). The dashed line is the designed trajectory and the solid line is the actual joint position.

their true values before having states convergence. In fact, the parameter estimates using the projection function $\mathcal{P}$ defined in [9] are never convergent. The use of high parameter update gains reduces the portion of the parameter uncertainties in the (Lyapunov-like) system non-negative function and allows each parameter estimate to change rapidly within its lower and upper bounds, aimed at suppressing state errors.

Remark 4.2: With respect to four different types of commercially available harmonic drives, experimental results are reported in terms of the maximum trajectory tracking errors in L_∞. For a more precise comparison, other norms in the sense of L_1 or L_2 might be required. Recently, a realistic benchmark problem for robust robot control was developed in [16].

VI. CONCLUSIONS

An adaptive joint torque controller that effectively compensates the large friction associated with harmonic drives, while incorporating the dynamics of the flexspline, is able to achieve asymptotic joint torque control. This adaptive joint torque controller has been extended to all the joints of a robot manipulator equipped with four different types of harmonic drives, and has been combined with a motion controller, namely the *virtual decomposition control*, to achieve precision motion control. Both individual joint motion and coordinated joint motion have been tested. Similar results for both motions at a moderate speed suggested the effectiveness of the *virtual decomposition control*. On the other hand, the effectiveness of the friction compensation was demonstrated by the ultra-precision motion control with encoder-resolution accuracy achieved at an ultra-low joint speed of 0.001 (rad/s). No stick-slip behavior was observed. Finally, it has to be pointed out that the precision control results reported in this paper require the measurements of both the motor and joint positions and the joint torque for each joint.

REFERENCES

[1] T. D. Tuttle and W. P. Seering, "A nonlinear model of a harmonic drive gear transmission," *IEEE Trans. Robotics and Automation*, vol. 12, no. 3, pp. 368-374, 1996.

[2] N. M. Kircanski and A. A. Goldenberg, "An experimental study of nonlinear stiffness, hysteresis, and friction effects in robot joints with harmonic drives and torque sensors," *Int. J. Robotics Research*, vol.16, no. 2, pp. 214-239, 1997.

[3] P. S. Gandhi, F. H. Ghorbel, and J. Dabney, "Modeling, identification, and compensation of friction in harmonic drives," *Proc. 41st IEEE Conference on Decision and Control*, vol. 1, pp. 160-166, 2002.

[4] R. Dhaouadi, F. H. Ghorbel, and P. S. Gandhi, "A new dynamic model of hysteresis in harmonic drives," *IEEE Transactions on Industrial Electronics*, vol. 50, no. 6, pp. 1165-1171, 2003.

[5] H. Kazerooni, "Dynamics and control of instrumented harmonic drives," *ASME J. Dyn. Syst., Meas., Control*, vol. 117, no. 1, 15-19, 1995.

[6] H. D. Taghirad and P. R. Belanger, "H_∞-based robust torque control of harmonic drive systems," *ASME. J. Dyn. Syst., Meas., and Control*, vol. 123, no. 3, pp. 338-345, 2001.

[7] W.-H. Zhu, Y.-G. Xi, Z.-J. Zhang, Z. Bien, and J. De Schutter, "Virtual decomposition based control for generalized high dimensional robotic systems with complicated structure," *IEEE Trans. Robotics and Automation*, vol. 13, no. 3, pp. 411-436, 1997.

[8] W.-H. Zhu and M. Doyon, "Adaptive control of harmonic drives," *Proc. of 43rd IEEE Conference on Decision and Control*, pp. 2602-2608, The Atlantis, Bahamas, December 2004.

[9] W.-H. Zhu and J. De Schutter, "Adaptive control of mixed rigid/flexible joint robot manipulators based on virtual decomposition," *IEEE Trans. Robotics and Automation*, vol. 15, no. 2, pp. 310-317, 1999.

[10] M. Hashimoto, "Robot motion control based on joint torque sensing," *Proc. of 1989 IEEE Int. Conf. Robotics and Automation*, pp. 256-261, 1989.

[11] M. Hashimoto, Y. Kiyosawa, and R. P. Paul, "A torque sensing technique for robots with harmonic drives," *IEEE Trans. Robotics and Automation*, vol. 9, no. 1, pp. 108-116, 1993.

[12] A. Albu-Schaffer and G. Hirzinger, "Parameter identification and passivity based joint control for a 7DOF torque controlled light weight robot," *Proc. of 2001 IEEE Int. Conf. Robotics and Automation*, pp. 2852-2858, Seoul, Korea, May 2001.

[13] A. De Luca, R. Farina, and P. Lucibello, "On the control of robots with visco-elastic joints," *Proc. of 2005 IEEE Int. Conf. Robotics and Automation*, pp. 4308-4313 (on-line pp. 4297-4302), Barcelona, Spain, April 2001.

[14] M. W. Spong, "Modeling and control of elastic joint robots," *ASME. J. Dyn. Syst., Meas., and Control*, vol. 109, pp. 310-319, 1987.

[15] R. Lozano and B. Brogliato, "Adaptive control of robot manipulators with flexible joints," *IEEE Trans. Automatic Control*, vol. 37, no. 2, pp. 174-181, 1992.

[16] S. Moberg and J. Ohr, "Robust control of a flexible manipulator arm: a benchmark problem," *Preprint of 16th IFAC World Congress*, Prague, July 2005.